

Premonitory earthquakes clustering process in an equivalent dimensions space before the Mw8.2 Tehuantepec, Mexico, 2017 mainshock

Stanislaw Lasocki¹, Vassilis G. Karakostas², F. Ramón Zúñiga³, and Eleftheria E. Papadimitriou⁴

¹Institute of Geophysics, Polish Academy of Sciences

²Geophysics Department, Aristotle University of Thessaloniki

³Universidad Nacional Autónoma de México

⁴Aristotle University of Thessaloniki

November 8, 2023

Abstract

A new approach to monitoring stochastic features of earthquake series was applied to track the preparatory process of the 2017 Tehuantepec, Mexico, Mw8.4 earthquake. The seismicity was parameterized by elapsed times and epicentral distances from the directly preceding earthquakes and by earthquake magnitudes. The transformation to equivalent dimensions ensured the comparability of these parameters. We were calculating the average distance between earthquakes in the transformed parameter space in moving in time data windows, each consisting of 100 events. The average distance exhibited a consistent upward trend from ten to two years before the main shock. Then, it declined until the main shock. This precursory up-down signal was highly significant statistically. We showed that the detected time changes of the average distance resulted from the evolution of the earthquake clustering in the considered parameters' equivalent dimensions space.

Hosted file

976851_0_art_file_11517326_s2zlyg.docx available at <https://authorea.com/users/561070/articles/674555-premonitory-earthquakes-clustering-process-in-an-equivalent-dimensions-space-before-the-mw8-2-tehuantepec-mexico-2017-mainshock>

Hosted file

976851_0_supp_11492210_s2883b.docx available at <https://authorea.com/users/561070/articles/674555-premonitory-earthquakes-clustering-process-in-an-equivalent-dimensions-space-before-the-mw8-2-tehuantepec-mexico-2017-mainshock>

1 **Earthquake parameters comparability** Premonitory earthquakes clustering process
2 **in an equivalent dimensions space before the Mw8.2 Tehuantepec, Mexico, 2017**
3 **mainshock**

4 **Stanisław Lasocki¹, Vasileios G. Karakostas², F. Ramón Zúñiga³, and Eleftheria E.**
5 **Papadimitriou²**

6 ¹Institute of Geophysics, Polish Academy of Sciences

7 ²Geophysics Department, Aristotle University of Thessaloniki

8 ³Instituto de Geofísica, Universidad Nacional Autónoma de México

9 Corresponding authors: Stanisław Lasocki (lasocki@igf.edu.pl)

10 **Key Points:**

- 11 • The average distance between earthquakes in the interevent time, interevent distance, and
12 magnitude space systematically changed in time.
- 13 • Statistically significant up-down trends of that distance occurred in the twelve years
14 preceding the mainshock.
- 15 • These premonitory changes resulted from the earthquake clustering process evolution.
16

17 **Abstract**

18 A new approach to monitoring stochastic features of earthquake series was applied to track the
19 preparatory process of the 2017 Tehuantepec, Mexico, Mw8.4 earthquake. The seismicity was
20 parameterized by elapsed times and epicentral distances from the directly preceding earthquakes
21 and by earthquake magnitudes. The transformation to equivalent dimensions ensured the
22 comparability of these parameters. We were calculating the average distance between
23 earthquakes in the transformed parameter space in moving in time data windows, each consisting
24 of 100 events. The average distance exhibited a consistent upward trend from ten to two years
25 before the mainshock. Then, it declined until the mainshock. This precursory up-down signal
26 was highly significant statistically. We showed that the detected time changes of the average
27 distance resulted from the evolution of the earthquake clustering in the considered parameters'
28 equivalent dimensions space.

29 **Plain Language Summary**

30 Despite intense research, so far, there are no methods, which decipher with usable confidence
31 that a seismic process leads to large and great earthquakes, and the problem awaits novel
32 approaches. We parameterized the seismicity preceding the 2017 Tehuantepec, Mexico, Mw8.4
33 earthquake by elapsed times and epicentral distances from the directly preceding events and
34 earthquake magnitudes. The transformation to equivalent dimensions, an innovative
35 methodology to investigate earthquake clustering, ensured the comparability of these parameters.
36 The average distance between earthquakes in the space of the transformed parameters exhibited a
37 consistent upward trend from ten to two years before the mainshock. Then it declined until the
38 mainshock. This highly significant statistically precursory up-down signal resulted from the
39 evolution of earthquake clustering in the used parameter space.

40 **1 Introduction**

41 Non-random, stochastic features of seismic series express the dynamics of seismic
42 processes. Identifying and deciphering these features significantly improve the capabilities for
43 earthquake forecasting. Commonly used earthquake parameters are the occurrence time,
44 epicenter location, hypocentral depth, and magnitude. Due to that, many studies of the
45 earthquake series non-randomness investigate stochastic properties – short- and long-range
46 clustering, memory, etc. of the series of occurrence times, locations, and magnitude, or derived
47 parameters – interoccurrence / interevent / recurrence time and interevent spatial distance.

48 In an early study of earthquake clustering in time, Gardner and Knopoff (1974), based on
49 the chi-square test results, concluded that earthquake series without aftershocks was Poissonian.
50 Kagan and Jackson (1991) drew the opposite conclusion based on investigations of interevent
51 time distribution in earthquake series deprived of short-term temporally clustered fragments.
52 However, the authors admitted that mainshocks' long-term clustering features were not readily
53 identifiable. Since then, much evidence of the persistence and long-term memory in the time
54 series of seismicity parameterizations has accumulated.

55 E.g., Corral (2004) compared the shapes of the earthquake recurrence time probability
56 densities for different spatial areas and magnitude ranges and indicated that the clustering
57 became self-similar in the localization–time–magnitude space after rescaling the time with the
58 event occurrence rate. Livina et al. (2005) showed that the interevent time was positively
59 correlated with the previous interevent time. Batac and Kantz (2014) found a certain threshold of

60 spatial separation of consecutive events. Events separated less than that threshold value were
61 correlated, while the more distant events were not. Moreover, the correlated events were
62 clustered in both time and space. Zhang et al. (2020) affirmed long-term memory for interevent
63 times and interevent distances from the estimates of lagged conditional density functions of these
64 parameters.

65 The Hurst exponent, H , parameterizes the long-term memory amount in a time series
66 (Hurst, 1951 and, e.g., Mandelbrot & Wallis, 1969). H estimated for the series of times between
67 consecutive earthquakes was often trending downward before moderate-strong earthquakes (Liu
68 et al., 1995). Studying H for the same parameterization Alvarez-Ramirez et al. (2012) indicated
69 that seismicity was clustered in time and the occurrences of more significant earthquakes were
70 positively correlated with H . The H estimates for the interevent time series, magnitude series,
71 and the series of inter-event epicentral distances of successive earthquakes in two different
72 seismogenic zones in Greece evidenced clustering in time and space in both areas, but the
73 magnitude series was internally correlated only in one (Gkarlaouni et al., 2017). H estimation
74 documented also a long-range memory in cumulative seismic moment series (Barani et al.,
75 2018).

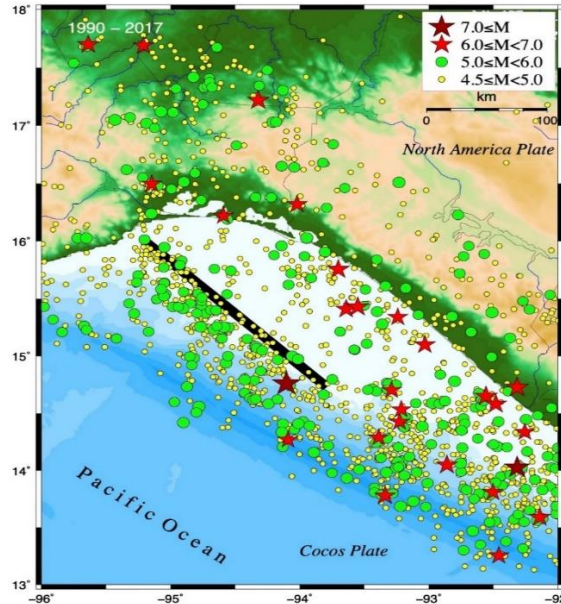
76 Whereas space-time clustering of earthquakes is generally accepted, the views on the
77 stochasticity of earthquake size (magnitude, seismic moment, energy) vary. In many studies, the
78 magnitude was considered memoryless and modeled by an exponential distribution resulting
79 from the Gutenberg-Richer relation (e.g., Kagan & Knopoff, 1981; Ogata, 1988; Sornette &
80 Helmstetter, 2002; Baiesi & Paczuski, 2004; Zaliapin et al., 2008; Zaliapin & Ben-Zion, 2013;
81 Batac et al., 2017; Michas et al., 2021), even though rigorous statistical tests undermined the
82 universality of the Gutenberg-Richter relation (Lasocki & Papadimitriou, 2006; Lasocki, 2007).
83 In recent years, however, there appeared studies evidencing the existence of memory in
84 magnitude series (e.g., Lennartz et al., 2008; Lippiello et al., 2008; Węglarczyk & Lasocki, 2009;
85 Gkarlaouni et al., 2017; Barani et al., 2018; 2021; Chen et al., 2022).

86 We studied the clustering of seismicity before the M8.2 Tehuantepec, Mexico,
87 earthquake. It occurred on September 8, 2017, at 04:49:18 (UTC) and is the largest intraslab
88 earthquake documented along the Mexican subduction zone.

89 The above-mentioned earthquake clustering studies indicate that interdependencies
90 among earthquakes in time and space are more easily discernible when examining interevent
91 times and interevent distances. For this reason, we parameterized the earthquakes from the 15
92 years before the M8.2 Tehuantepec earthquake by these two parameters and magnitudes. We
93 transformed these parameters to equivalent dimensions (Lasocki, 2014) to get the Euclidean
94 distance function in their 3D space. Then, in time-moving data windows, we calculated the
95 average distance between the earthquakes in this space, and we found statistically significant
96 time trends of this distance, which preceded the mainshock.

97 **2 Data and Methods**

98 The M8.2 Tehuantepec earthquake from September 8, 2017 exhibited normal faulting
 99 (Melgar et al., 2018; Suárez et al., 2019) within the subducting Cocos Plate ~70 km landward
 100 (Ye, et al., 2017) from the Middle American Trench beneath the Tehuantepec gap (Kelleher, et
 101 al., 1973; Kelleher & McCann, 1976) (Figure 1).



102
 103 *Figure 1. The study area where the epicentral distribution of earthquakes that occurred from 1990 – 2017 is shown. Different*
 104 *symbols show different magnitude ranges, as indicated in the legend. The thick black line shows the inferred surface extension of*
 105 *the main rupture.*

106 The study area is bounded between 13°-18° N and 92°-96°W, with its length along the
 107 subduction front taken about three times the fault length of the 2017 rupture. We used the data
 108 since 1999 from the earthquake catalog compiled by the Universidad Nacional Autónoma de
 109 México, whose magnitudes were homogeneously calculated (Zúñiga et al., 2000). Because the
 110 selected data exhibited a sharp, physically unjustified increase of the event occurrence rate that
 111 began in 2015 but concerned only smaller events of magnitudes up to 4.5, we decided to use
 112 earthquakes of $M > 4.5$. The studied dataset comprised 1048 events and the mainshock within this
 113 earthquake series was event #1049. The earthquakes were parameterized by the occurrence time,
 114 focal latitude, longitude and depth, and magnitude.

115 We re-parameterized these earthquakes by the occurrence time, t , magnitude, M , and the
 116 interevent time, dt , and orthodromic epicentral distance (interevent distance), dr , between this
 117 event and the preceding event. The re-parameterized series comprised 1047 earthquakes.
 118 Subsequently, we transformed the dt , dr , and M into their equivalent dimensions (EDs), DT , DR ,
 119 and MC , respectively.

120 The transformation to EDs (Lasocki, 2014; 2021), based on a probabilistic equivalence of
 121 parameters of objects under study, replaces parameter values with their cumulative distribution
 122 function (CDF) values. Unknown CDF-s are estimated from data using the non-parametric
 123 kernel estimators. We used the data of all 1047 earthquakes under study to estimate the CDF-s of

124 dt , dr , and M (See: Supporting Information Text S1 on the transformation applied in the present
125 work).

126 All parameters transformed to EDs are uniformly distributed in $[0, 1]$, hence comparable,
127 and the space of ED-transformed parameters has the Euclidean metric. After the transformation,
128 the earthquakes became points $[DT, DR, MC]$ in the 3D cube $[0, 1]$.

129 From the Euclidean metric of ED-s spaces, it comes that the average distance between n
130 earthquakes in the $\{DT, DR, MC\}$ space reads

$$131 \quad d_c = \frac{2}{(n-1)n} \sum_{k=1}^{n-1} \sum_{j=k+1}^n D(k, j) =$$

$$132 \quad \frac{2}{(n-1)n} \sum_{k=1}^{n-1} \sum_{j=k+1}^n \sqrt{(DT_k - DT_j)^2 + (DR_k - DR_j)^2 + (MC_k - MC_j)^2}. \quad (1)$$

133 Starting with event #8, we overlaid the event series 10–1047 with 48 windows of 100
134 consecutive events each, being shifted by 20 events, and calculated d_c in windows. Unless the
135 event generation process is stationary and ergodic, taking parameters of n consecutive events
136 from a time series of N events, $n < N$, is a non-random draw. Therefore, while in the population of
137 all data, the transformed parameters, DT , DR , and MC , were uniformly distributed in $[0, 1]$, their
138 distributions in the sliding window were not and were changeable, likewise d_c , reflecting the
139 earthquake process's properties in the window's period. We linked d_c -s to the occurrence times of
140 the last events in the windows obtaining the 48-element time series $d_c(t)$.

141 The statistical significance of non-random features of $d_c(t)$ was studied in two ways.
142 First, we calculated d_c -values in 100,000 samples of size 100, each randomly drawn from the
143 initial series of $[DT, DR, MC]$ triples from #8 to #1047 obtaining the empirical distribution of
144 $\{d_c | \text{random sampling of } [DT, DR, MC] \text{ triples}\}$. From this distribution, we estimated the p_α and
145 $p_{1-\alpha}$ percentiles of d_c .

146 If a series of d_c comprises n values that were calculated from randomly drawn triples
147 $[DT, DR, MC]$, the probability that k values $> p_\alpha$ equals the probability that k values $< p_{1-\alpha}$ and is:

$$148 \quad \Pr(n, k, p_\alpha) = 1 - \sum_{m=0}^{k-1} \binom{n}{m} (1 - \alpha)^m \alpha^{n-m}. \quad (2)$$

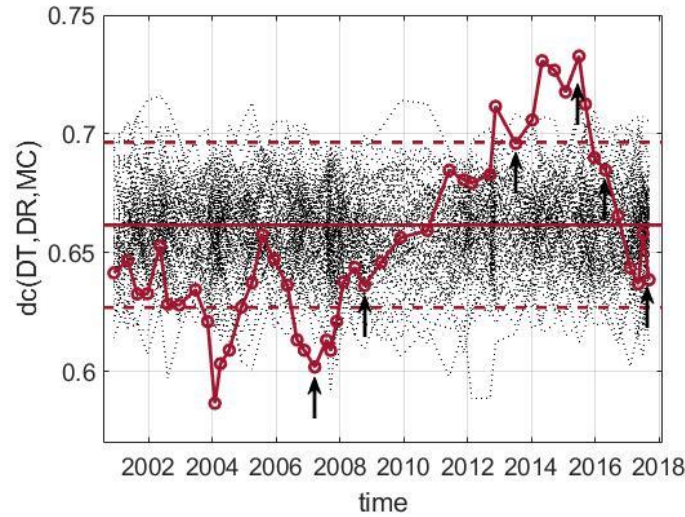
149 Using the significance $\alpha=0.995$ we counted the number of times, k , the $d_c(t)$ -values were
150 greater than p_α / less than $p_{1-\alpha}$ and applied Eq. 2 to calculate $\Pr(48, k, p_{0.995}) / \Pr(48, k, p_{0.005})$.

151 In the second test, we shuffled a hundred times the original series of triples $[DT_k, DR_k,$
152 $MC_k]$, $k=1, \dots, 1047$. Then, using windows of 100 triples consecutive in shuffled series and
153 sliding them by 20 triples, we calculated one hundred $d_c(t | \text{shuffled series of } [DT, DR, MC]$
154 $\text{triples})$ series and compared qualitatively their shapes with the shape of actual $d_c(t)$ series.

155

156 **3 Results and Discussion**

157 The obtained time series of the average distances between earthquakes in the consecutive
 158 data windows, $d_c(t)$, is shown in Figure 2. From $d_c=0.64$ in window #20, attributed to 20 March
 159 2007, $d_c(t)$ increases systematically until 28 June 2015 ($d_c=0.78$). Afterward, the trend of $d_c(t)$
 160 exhibits a rapid decline, which continues from 6 May 2017 ($d_c=0.68$) to 7 September 2017
 161 ($d_c=0.68$). The mainshock occurred on 8 September 2017.



162

163 *Figure 2. Time series of the average distance in the {DT, DR, MC} space between a hundred consecutive earthquakes.*
 164 *Horizontal solid - the mean d_c for one hundred perfectly unclustered [DT, DR, MC] points. Dashed lines - the 90-per cent*
 165 *confidence interval of d_c for a single draw of unclustered points. Dotted lines - one hundred d_c -series obtained from the shuffled*
 166 *[DT, DR, MC] triples. Arrows - the points on $d_c(t)$ used for an insight into the evolution of earthquake clustering.*

167 From the empirical distribution of $\{d_c | \text{random sampling of [DT, DR, MC] triples}\}$
 168 obtained from 100,000 draws, we established the 0.005 and 0.995 percentiles to be $p_{0.005}=0.6141$
 169 and $p_{0.995}=0.7041$. In the $d_c(t)$ series, seven values were greater than $p_{0.995}$ and eight values were
 170 less than $p_{0.005}$. These results yielded highly low probabilities, $\text{Pr}(48,7, p_{0.995}) = 4.81 \times 10^{-9}$
 171 and $\text{Pr}(48,8, p_{0.005}) = 1.23 \times 10^{-10}$, for the thesis that the peaks of $d_c(t)$ were due to the
 172 statistical scatter of d_c obtained from random triples [DT, DR, MC].

173 However, due to the overlaps of windows in which we calculated $d_c(t)$, these d_c -s were
 174 correlated. Consequently, the probabilities $\text{Pr}(48,7, p_{0.995})$ and $\text{Pr}(48,8, p_{0.005})$ were not as from
 175 Eq. (2). To study the consequences of the window overlaps, we used the one hundred
 176 $d_c(t)$ shuffled series of [DT, DR, MC] triples series (see: Data and Methods), counting in each
 177 series the number of times its values were greater than $p_{0.995}$ / less than $p_{0.005}$. Proportions of the
 178 $d_c(t)$ shuffled series of [DT, DR, MC] triples series in which d_c -values were greater/less than
 179 $p_{0.995}/p_{0.005}$ $k=1, 2, 3, 4, 5$ times are compared with the respective probabilities from Eq. (2) in
 180 Table 1.

181 For $k>1$, the non-zero proportions are greater than the respective probabilities for truly
 182 randomly drawn triples [DT, DR, MC]. A very rough estimate of a multiplication factor of this
 183 probability increase is 10^{k-1} . If so, the probability of a random origin of the number of times that
 184 $d_c(t)$ exhibits the values above/below $p_{0.995}/p_{0.005}$ would still be on the order of 10^{-3} . Furthermore,
 185 the maximum number of instances where the values of $d_c(t)$ shuffled series of [DT, DR, MC]

186 *triples*) series deviated from the interval $[p_{0.005}, p_{0.995}]$ was six. In contrast, the original $d_c(t)$
187 series had fifteen instances where its values fell outside this interval.
188

189
190Table 1. Comparison of the shuffled series proportions, in which d_c -values k times were outside $[p_{0.005}, p_{0.995}]$, with the probability of such cases according to Eq. (2).

k	Proportion of $d_c(t shuffled\ series\ of\ [DT, DR, MC]\ triples)$ in which at least k -times:		$\Pr(48, k, p_{0.995}) = \Pr(48, k, p_{0.005})$ (Eq. (2))
	$d_c - values \geq p_{0.995}$	$d_c - values \leq p_{0.005}$	
1	0.17	0.22	0.214
2	0.08	0.06	0.024
3	0.02	0.02	0.0018
4	0.02	0	0.0001
5	0	0	0.000004

191

192

193

194

195

196

We also took every fifth window. Such windows do not overlap and the probability that random scatter caused d_c -values to be outside the range is as in Eq. (2). The respective $d_c(t)$ series consisted of ten elements. In this series, there were two d_c -s greater than $p_{0.995}$ and two d_c -s less than $p_{0.05}$. According to Eq. (2), the probability to get such results at random was $\Pr(10,2,p_{0.995}) = \Pr(10,2,p_{0.005}) = 0.0011$.

197

198

199

200

201

Not only the extreme amplitudes, non-random as shown above, are characteristic of $d_c(t)$, but also the shape of $d_c(t)$ from March 2007 to the mainshock. This shape is compared in Figure 2 with the shapes of the one hundred $d_c(t|shuffled\ series\ of\ [DT, DR, MC]\ triples)$ series (dotted lines). The $d_c(t)$ series clearly differs from all $d_c(t|shuffled\ series\ of\ [DT, DR, MC]\ triples)$ series in the trends' lengths and widths of peaks.

202

203

204

205

206

The minimum achievable value of d_c - the average distance between earthquakes in $\{DT, DR, MC\}$ space, is zero. In such a case, the earthquake process is perfectly regular: interevent time and distance are constant, and magnitudes are the same. Earthquakes are clustered in one point in the $\{DT, DR, MC\}$ space. In this context, a d_c increase reflects the diminishing regularity of the earthquake process.

207

208

209

210

211

212

213

214

Having $8 \times N$ points in the $[0, 1] \{DT, DR, MC\}$ cube, d_c becomes maximum if there are N points at each cube vertex. For 96 points (8×12), this maximum of $d_c=1.13364$. For 100 points, the d_c takes the maximum when 96 points are distributed among eight vertices of the cube in equal parts, and the separation of the remaining four points is maximum, e.g., they are located at $(0,0,0)$, $(1,1,1)$, $(0,1,0)$, $(1,0,1)$ or the like. For that distribution, $d_c=1.13303$. Hence in case of one hundred earthquakes windows, an increase of d_c from zero to 1.13303 means moving from a one-point cluster to eight best-balanced and maximally distant one-point clusters. On the way, there is a perfectly unclustered state.

215

216

217

218

Points-earthquakes are unclustered in $[0, 1]$ cube when their components, $[DT, DR, MC]$, are drawn from the three-dimensional standard uniform distribution. To get properties of the unclustered state, we drew one million samples, one hundred elements each, from this distribution. Based on this data, we have established that:

219

220

- The mean mass center of the unclustered points is at $(0.5, 0.5, 0.5)$, and the standard deviation of this location is $(0.0289, 0.0289, 0.0289)$ with a precision of 10^{-5} ;

- 221 • The mean sum of distances from such one hundred points to their mass center is 48.03,
 222 with a standard deviation of 1.39;
 223 • The mean value of one million d_c values is $\langle d_c \rangle = 0.661714$, and the standard deviation is
 224 $\sigma = 0.017731$. Hence, the 90-percent confidence interval of a single draw is (0.626960;
 225 0.696467). The mean value and the 90-percent confidence interval limits for a single
 226 draw are marked in Figure 2 by the horizontal solid and two dashed lines, respectively.

227 The part of the $d_c(t)$ curve from March 2007 to the mainshock (8/09/2017) begins
 228 significantly below $\langle d_c \rangle$, then crosses $\langle d_c \rangle$ and increases to values significantly above $\langle d_c \rangle$
 229 (Figure 2). Next, it goes down again below $\langle d_c \rangle$. This behavior suggests that the earthquakes in
 230 windows linked to smaller $d_c(t)$ values may have tended to form one cluster, and those in
 231 windows linked to greater $d_c(t)$ values may have built more than one cluster.

232 To look closer at the evolution of earthquake clustering, we took the data from six data
 233 windows linked to the points marked by arrows in Figure 2. Out of these six, only two windows,
 234 No.s 4 and 5, partially overlapped. We estimated the optimal number of clusters in every
 235 window. Because the problem of dividing points into clusters is equivocal, different optimality
 236 criteria provide different clustering results. Out of the five tested criteria (See: Supporting
 237 Information Text S2 for the choice of the optimal number of clusters criterion), we used the gap
 238 criterion with the PCA reference data generation method (Tibshirani et al., 2001). The accepted
 239 “optimal” numbers of data clusters in the studied windows, the division of earthquakes in the
 240 windows into the clusters, and the coordinates of the resultant clusters’ centroids are shown in
 241 Table 2.

242 The window #1 mass center was at (0.51, 0.54, 0.45). Hence, the probability that the
 243 deviations of window #1 mass center components from 0.5 were due only to statistical scatter are
 244 0.365, 0.083, 0.042, respectively, and the probability that the mass center deviated from the point
 245 (0.5, 0.5, 0.5) due to statistical scatter is 1.3×10^{-3} . The total distance of the points in windows #1
 246 to their mass centers was 43.18. The probability that a single draw of one hundred unclustered
 247 points would provide this distance value is 2.4×10^{-4} .

248 The window #6 mass center was at (0.45, 0.46, 0.53). The probabilities that only
 249 statistical scatter caused the deviations of mass center components from 0.5 and the mass center
 250 deviation from (0.5, 0.5, 0.5) are 0.042, 0.083, 0.150, and 5.2×10^{-4} , respectively. The total
 251 distance of window #6 points to the mass center was 45.85. The probability that such a result
 252 would be obtained for an unclustered points draw is 0.058.

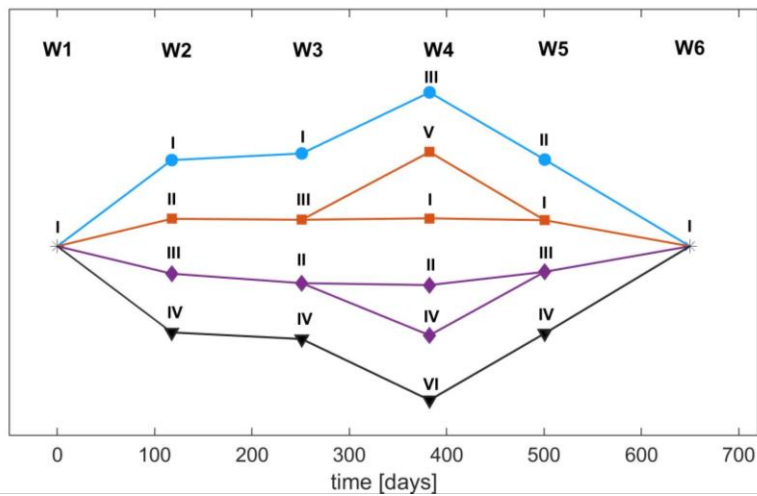
253 These results indicate that the points in windows #1 and #6 were not unclustered but built
 254 single clusters. This fact and the results from Table 2 suggest that the up-down trends of $d_c(t)$
 255 preceding the Tehuantepec mainshock resulted from the following earthquake clustering process
 256 in the $\{DT, DR, MC\}$ [0, 1] cube. At the beginning (18/08/2005 – 20/03/2007), the earthquakes
 257 formed one cluster. The decay of this cluster in separate groups – four in windows #2 and #3
 258 increased $d_c(t)$. The maximum $d_c(t)$ was linked to separating of one hundred earthquakes into as
 259 many as six clusters. Next, the number of clusters was gradually reduced – four clusters in
 260 window #5 and only one in the last window before the mainshock (window #6). This decrease in
 261 clusters caused the systematic decrease of $d_c(t)$. The centroids' coordinates from Table 2 suggest
 262 that this clustering process could schematically look like in Figure 3.

263
264
265
266
267

Table 2. Results of the division of earthquakes in windows into the optimal number of clusters. Centroid coordinates for ‘all data’ cases refer to the mass centers of all points in windows.

No.	Window time point, t	$d_c(t)$	Optimal number of clusters	Cluster No	Centroid coordinates			Number of cluster members
					DT	DR	MC	
1	20/03/2007	0.601	1	I	0.51	0.54	0.45	100
2	9/10/2008	0.636	4	I	0.15	0.19	0.37	25
				II	0.75	0.34	0.34	21
				III	0.41	0.77	0.17	25
				IV	0.38	0.59	0.73	29
3	4/07/2013	0.696	4	I	0.15	0.17	0.72	29
				II	0.63	0.59	0.22	22
				III	0.83	0.30	0.79	24
				IV	0.55	0.80	0.77	25
4	28/06/2015	0.733	6	I	0.40	0.16	0.25	13
				II	0.34	0.86	0.24	14
				III	0.16	0.18	0.73	21
				IV	0.85	0.71	0.27	16
				V	0.76	0.36	0.82	22
				VI	0.52	0.85	0.85	14
5	27/04/2016	0.685	4	I	0.53	0.21	0.22	20
				II	0.16	0.20	0.74	19
				III	0.52	0.77	0.22	29
				IV	0.67	0.55	0.82	32
6	7/09/2017	0.639	1	I	0.45	0.46	0.53	100

268



269

Figure 3. The proposed scheme of the earthquake clustering process preceding the Tehuantepec M8.2 mainshock. W1-W6 mark windows, and roman numbers denote the windows’ clusters as in Table 2. The windows locations on time axis agree with periods between times of the windows’ middles. The vertical separations of the nodes/clusters in the same window are proportional to the distance between centroids of neighboring nodes.

274

275 **4 Conclusions**

276 The re-parameterization of seismicity into interevent times and distances and the use of
277 the transformation to equivalent dimensions to ensure comparability of parameters shed new
278 light on the preparatory process to the Tehuantepec earthquake. The average distance between
279 earthquakes in the space of equivalent: interevent time, interevent distance, and magnitude time
280 series exhibited distinct and systematic time changes. Its part from March 2007 until the
281 mainshock (9/09/2017) was a statistically significant precursory signal. This signal included a
282 well-developed rise from March 2007 to June 2015, followed by a decrease until the mainshock.
283 These premonitory changes were linked to the earthquake clustering process evolution. Further
284 research across other great earthquake cases will determine the usefulness of the approach
285 presented here in the earthquake forecasting problem.

286 **Acknowledgments**

287 The work was supported by a subsidy from the Polish Ministry of Education and Science
288 for the Institute of Geophysics, Polish Academy of Sciences, and Project no. 2021/WK/09
289 subsidized by the Polish Ministry of Education and Science.
290

291 **Open Research**

292 Data used in this work is the catalogue from the Mexican Seismological Service of
293 Mexico, SSN (2023): Universidad Nacional Autónoma de México, Instituto de Geofísica,
294 Servicio Sismológico Nacional, México: <http://www2.ssn.unam.mx:8080/catalogo/>. The
295 transformation to equivalent dimensions was done using the Transformation to Equivalent
296 Dimensions application (Leptokaropoulos et al., 2020), available as an application implemented
297 on the EPISODES platform - <https://EpisodesPlatform.eu> (Orlecka et al., 2020).
298

299 **References**

- 300 Baiesi, M., & Paczuski, M. (2004). Scale-free networks of earthquakes and aftershocks. *Physics*
301 *Review E*, 69, 066106. doi: 10.1103/PhysRevE.69.066106
- 302 Barani, S., Mascandola, C., Riccomagno, E., Spallarossa, D., Albarello, D., Ferretti, G., Scafidi,
303 D., Augliera, P., & Massa, M. (2018). Long-range dependence in earthquake-moment release
304 and implications for earthquake occurrence probability. *Scientific Reports*, 8, 5326. doi:
305 10.1038/s41598-018-23709-4.
- 306 Barani, S., Cristofaro, L., Taroni, M., Gil-Alaña, L.A., & Ferretti, G. (2021). Long memory in
307 earthquake time series: the case study of the Geysers Geothermal Field. *Frontiers of Earth*
308 *Science*, 9, 563649. doi: 10.3389/feart.2021.563649
- 309 Batac, R.C., & Kantz, H. (2014). Observing spatio-temporal clustering and separation using
310 interevent distributions of regional earthquakes. *Nonlinear Process in Geophysics*, 21, 735–744.
311 doi: 10.5194/npg-21-735-2014

- 312 Batac, R.C., Paguirigan Jr., A.A., Tarun, A.B., & Longjas, A.G. (2017). Sandpile-based model
 313 for capturing magnitude distributions and spatiotemporal clustering and separation in regional
 314 earthquakes. *Nonlinear Process in Geophysics*, 24, 179–187. doi: 10.5194/npg-24-179-2017
- 315 Calinski, T., & Harabasz, J. (1974). A Dendrite Method for Cluster Analysis. *Communications in*
 316 *Statistics. Theory and Methods*, 3, 1-27. doi: 10.1080/03610927408827101
- 317 Chen, Ku-Cheng., Kim, K-H., Wang, J-H., & Chen, Kuo-Chang (2022). Dominant periods and
 318 memory effect of the 2021 earthquake swarm in Hualien, Taiwan. *Terrestrial Atmospheric*
 319 *Oceanic Sciences*, 33, 24, doi: 10.1007/s44195-022-00022-2
- 320 Corral, Á. (2004). Long-term clustering, scaling, and universality in the temporal occurrence of
 321 earthquakes. *Physics Review Letters*, 92 (10), 108501. doi:10.1103/PhysRevLett.92.108501
- 322 Davies, D.L., & Bouldin, D.W. (1979). A Cluster Separation Measure. in *IEEE Transactions on*
 323 *Pattern Analysis and Machine Intelligence*, vol. PAMI-1, no. 2, 224-227, doi:
 324 10.1109/TPAMI.1979.4766909.
- 325 Gardner, J.K., & Knopoff, L. (1974). Is the sequence of earthquakes in southern California, with
 326 aftershocks removed, Poissonian? *Bulletin Seismological Society America*, 64, 1363-1367. doi:
 327 10.1785/BSSA0640051363
- 328 Gkarlaouni, C., Lasocki, S., Papadimitriou, E., & Tsaklidis, G. (2017). Hurst analysis of
 329 seismicity in Corinth rift and Mygdonia graben (Greece). *Chaos, Solitons and Fractals*, 96, 30–
 330 42. doi: 10.1016/j.chaos.2017.01.001
- 331 Hurst, H. E. (1951). Long-Term Storage Capacity of Reservoirs. *Transactions American Society*
 332 *Civil Engineers*, 116, 770-799. doi: 10.1061/TACEAT.0006518
- 333 Kagan, Y.Y., & Jackson, D.D. (1991). Long-term earthquake clustering. *Geophysical Journal*
 334 *International*, 104, 117-133. doi: 10.1111/j.1365-246X.1991.tb02498.x
- 335 Kagan, Y.Y., & Knopoff, L. (1981). Stochastic synthesis of earthquake catalogs. *Journal*
 336 *Geophysical Research*, 86 (B4), 2853-2862. doi: 10.1029/JB086iB04p02853
- 337 Kelleher, J. A., & McCann, W. R. (1976). Buoyant zones, great earthquakes, and unstable
 338 boundaries of subduction. *Journal Geophysical Research*, 81, 4885–4896. doi:
 339 10.1029/JB081i026p04885
- 340 Kelleher, J. A., Sykes, L. R., & Oliver, J. (1973). Possible criteria for predicting earthquake
 341 locations and their applications to major plate boundaries of the Pacific and Caribbean region.
 342 *Journal Geophysical Research*, 78, 2547–2585. doi: 10.1029/JB078i014p02547
- 343 Lasocki, S. (2007). Evidences of complexity of magnitude distribution obtained from a non-
 344 parametric testing procedure, in *Proceedings of the 5th International Workshop of Statistical*
 345 *Seismology “Physical and Stochastic Modelling of Earthquake Occurrence and Forecasting”*
 346 (StatSei 5), Erice, Italy.
- 347 Lasocki, S. (2014). Transformation to equivalent dimensions – a new methodology to study
 348 earthquake clustering. *Geophysical Journal International*, 197 (2), 1224-1235. doi:
 349 10.1093/gji/ggu062

- 350 Lasocki, S. (2021). Kernel Density Estimation in Seismology. Chapter 1 in Statistical Methods
351 and Modelling of Seismogenesis, Limnios, N., Papadimitriou, E., Tsaklidis, G., eds., ISTE,
352 Wiley, pp. 1-26.
- 353 Lasocki, S., & Papadimitriou, E. E. (2006). Magnitude distribution complexity revealed in
354 seismicity from Greece. *Journal Geophysical Research*, 111, B11309, doi:
355 10.1029/2005JB003794
- 356 Lennartz, S., Livina, V.N., Bunde, A., & Havlin, S. (2008). Long-term memory in earthquakes
357 and the distribution of interoccurrence times. *Earth Planetary Letters*, 81, 69001. doi:
358 10.1209/0295-5075/81/69001
- 359 Leptokaropoulos, K., Lasocki, S., & Urban, P. (2020) Transformation to Equivalent Dimensions
360 (version September 2020) [Software]. <https://episodesplatform.eu/?lang=en#app:T2ED>
- 361 Lippiello, E., de Arcangelis, L., & Godano, C. (2008). Influence of time and space correlations
362 on earthquake magnitude. *Physics Review Letters*, 100, 038501, doi:
363 10.1103/PhysRevLett.100.038501
- 364 Liu, CH., Liu, YG., & Zhang, J. (1995). R/S analysis of earthquake time interval. *Acta*
365 *Seismologica Sinica*, 8, 481–485. doi: 10.1007/BF02650577
- 366 Livina, V. N., Havlin, S., Bunde, A. (2005). Memory in the occurrence of earthquakes. *Physics*
367 *Review Letters*, 95, 208501. doi: 10.1103/PhysRevLett.95.208501
- 368 Mandelbrot, B., & Wallis, J. (1969). Robustness of the rescaled range R/S in the measurement of
369 noncyclic long run statistical dependence. *Water Resources Research*, 5, 967-988, doi:
370 10.1029/WR005i005p00967.
- 371 Melgar, D., Ruiz-Angulo, A., Garcia, E. S., Manea, M., Manea, V. C., Xu, X., et al. (2018).
372 Deep embrittlement and complete rupture of the lithosphere during the M8.2 Tehuantepec
373 earthquake. *Nature Geoscience*. doi: 10.1038/s41561-018-0229-y
- 374 Michas, G., Kapetanidis, V., Kaviris, G., & Vallianatos, F. (2021). Earthquake diffusion
375 variations in the Western Gulf of Corinth (Greece). *Pure Applied Geophysics*, 178, 2855–2870.
376 doi: 10.1007/s00024-021-02769-0
- 377 Ogata, Y. (1988). Statistical models for earthquake occurrences and residual analysis for point
378 processes. *Journal of the American Statistical Association*, 83 (401), 9-27. doi:
379 10.1080/01621459.1988.10478560
- 380 Orlecka-Sikora B., Lasocki S., Kocot J., Szepieniec T., Grasso J-R., Garcia-Aristizabal A., et al.,
381 (2020). An open data infrastructure for the study of anthropogenic hazards linked to georesource
382 exploitation. *Scientific Data* 7, 89. doi:10.1038/s41597-020-0429-3
- 383 Rousseeuw, P.J. (1987) Silhouettes: A graphical aid to the interpretation and validation of cluster
384 analysis. *Journal of Computational and Applied Mathematics*, 20, 53-65. doi: 10.1016/0377-
385 0427(87)90125-7
- 386 Silverman, B. W. (1986). *Density Estimation for Statistics and Data Analysis*. Chapman and
387 Hall, London, pp. 176.

- 388 Sornette, D., & Helmstetter, A. (2002). Occurrence of finite-time singularities in epidemic
389 models of rupture, earthquakes, and starquakes. *Physics Review Letters*, 89 (15), 158501. doi:
390 10.1103/PhysRevLett.89.158501
- 391 Suárez, G., Santoyo, M. A., Hjorleifsdottir, V., Iglesias, A., Villafuerte, C., & Cruz–Atienza, V.
392 M. (2019). Large scale lithospheric detachment of the downgoing Cocos plate: The 8 September
393 2017 earthquake (Mw8.2). *Earth Planetary Science Letters*, 509, 9–14. doi:
394 10.1016/j.epsl.2018.12.018
- 395 Tibshirani, R., Walther, G. & Hastie, T. (2001). Estimating the number of clusters in a data set
396 via the gap statistic. *Journal Royal Statistical Society: Series B (Statistical Methodology)*, 63,
397 411-423. doi: 10.1111/1467-9868.00293
- 398 Węglarczyk, S., & Lasocki, S. (2009) Studies of short and long memory in mining-induced
399 seismic processes. *Acta Geophysica*, 57, 696-715. doi: 10.2478/s11600-009-0021-x
- 400 Ye, L., Lay, T., Bai, Y., Cheung, K. F., & Kanamori, H. (2017). The 2017 Mw 8.2 Chiapas,
401 Mexico, earthquake: Energetic slab detachment. *Geophysical Research Letters*, 44, 11,824–
402 11,832. doi: 10.1002/2017GL076085
- 403 Zaliapin, I., & Ben-Zion, Y. (2013), Earthquake clusters in southern California I: Identification
404 and stability. *Journal Geophysical Research*, 118, 2847–2864. doi: 10.1002/jgrb.50179
- 405 Zaliapin, I., Gabrielov, A., Keilis-Borok, V., & Wong, H. (2008). Clustering analysis of
406 seismicity and aftershock identification. *Physics Review Letters* 101, 018501. doi:
407 10.1103/PhysRevLett.101.018501
- 408 Zhang, Y., Fan, J., Marzocchi, W., Shapira, A., Hofstetter, R., Havlin, S., & Ashkenazy, Y.
409 (2020). Scaling laws in earthquake memory for interevent times and distances. *Physis Review*
410 *Research*, 2, 013264. doi: 10.1103/PhysRevResearch.2.013264
- 411 Zúñiga, F. R., Reyes, M. A., & Valdés, C. (2000). A general overview of the catalog of recent
412 seismicity compiled by the Mexican Seismological Survey. *Geofísica Internacional*, 39, 161–
413 170. doi: 10.22201/IGEOF.00167169P.2000.39.2.273
414